BIOLOGICAL CRYSTALLOGRAPHY
ISSN 1399-0047

Structural insights into the novel inhibition mechanism of *Trypanosoma cruzi* spermidine synthase

Yasushi Amano,* Ichiji Namatame, Yukihiro Tateishi, Kazuya Honboh, Eiki Tanabe, Tatsuya Niimi and Hitoshi Sakashita

Drug Discovery Research, Astellas Pharma Inc., 21 Miyukigaoka, Tsukuba, Ibaraki 305-8585, Japan. *Correspondence e-mail: yasushi-amano@astellas.com

Received 23 March 2015
Accepted 7 July 2015

Edited by K. Miki, Kyoto University, Japan

Keywords: spermidine synthase; *Trypanosoma cruzi*; fragment-based drug discovery; Chagas disease; allosteric inhibition.

PDB references: spermidine synthase, complex with decarboxylated *S*-adenosylmethionine, 4yuv; complex with *trans*-4-methylcyclohexylamine, 4yuw; complex with 2*H*-1,4-benzothiazin-3-amine, 4yux; complex with isoquinolin-1-amine, 4yuy; complex with 5-[(4-methylbenzyl)oxy]quinazoline-2,4-diamine, 4yuz; complex with *N*-methyl-*N*-phenyl-2,3-dihydro-1,4-benzodioxine-2-carboxamide, 4yu0; complex with quinolin-8-yl piperidine-1-carboxylate, 4yu1; complex with 2-phenyl-1,2-thiazol-3(2*H*)-one, 4yu2

Supporting information: this article has supporting information at journals.iucr.org/d

Trypanosoma cruzi causes Chagas disease, a severe disease affecting 8–10 million people in Latin America. While nifurtimox and benznidazole are used to treat this disease, their efficacy is limited and adverse effects are observed. New therapeutic targets and novel drugs are therefore urgently required. Enzymes in the polyamine–trypanothione pathway are promising targets for the treatment of Chagas disease. Spermidine synthase is a key enzyme in this pathway that catalyzes the transfer of an aminopropyl group from decarboxylated *S*-adenosylmethionine (dcSAM) to putrescine. Fragment-based drug discovery was therefore conducted to identify novel, potent inhibitors of spermidine synthase from *T. cruzi* (TcSpdSyn). Here, crystal structures of TcSpdSyn in complex with dcSAM, *trans*-4-methylcyclohexylamine and hit compounds from fragment screening are reported. The structure of dcSAM complexed with TcSpdSyn indicates that dcSAM stabilizes the conformation of the 'gate-keeping' loop to form the putrescine-binding pocket. The structures of fragments bound to TcSpdSyn revealed two fragment-binding sites: the putrescine-binding pocket and the dimer interface. The putrescine-binding pocket was extended by an induced-fit mechanism. The crystal structures indicate that the conformation of the dimer interface is required to stabilize the gatekeeping loop and that fragments binding to this interface inhibit TcSpdSyn by disrupting its conformation. These results suggest that utilizing the dynamic structural changes in TcSpdSyn that occur upon inhibitor binding will facilitate the development of more selective and potent inhibitors.

1. Introduction

Neglected tropical diseases (NTDs) are infectious diseases caused by protozoa, helminths, viruses or bacteria that primarily affect poor populations in tropical countries. NTDs affect more than one billion people worldwide and worsen and prolong poverty (Centers for Disease Control and Prevention, 2011). The World Health Organization (WHO) has prioritized 17 NTDs endemic in 149 countries and coordinates policies and strategies for the control of these diseases (World Health Organization, 2013). Of these 17 NTDs, Chagas disease, caused by *Trypanosoma cruzi*, is endemic in Latin America and affects 8–10 million people (World Health Organization, 2015; Centers for Disease Control and Prevention, 2013). While nifurtimox and benznidazole are currently used for the treatment of Chagas disease, these drugs exhibit limited and varied efficacy and cause adverse effects (Bern *et al.*, 2007).

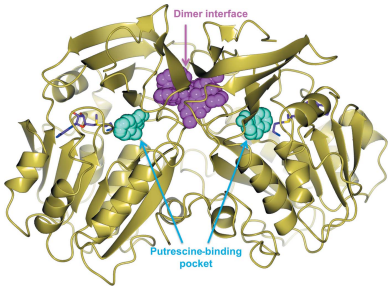

The polyamine–trypanothione pathway has been the focus of recent study as a drug target of trypanosomes and leishmanias (Maya *et al.*, 2014; Colotti *et al.*, 2013). Trypanothione [N^1,N^8-bis(glutathionyl)spermidine] is an essential metabolite found in trypanosomes and leishmania but not in mammals (Fairlamb *et al.*, 1985) that protects against oxidative stress (Flohé *et al.*, 1999; Krauth-Siegel & Comini, 2008; Manta *et al.*, 2013). Inhibition of the polyamine–trypanothione pathway is therefore a promising strategy for treating Chagas disease.

Of the key proteins in the polyamine–trypanothione pathway, spermidine synthase (SpdSyn) catalyzes the transfer of the aminopropyl group from decarboxylated *S*-adenosylmethionine (dcSAM) to putrescine to generate spermidine (Ikeguchi *et al.*, 2006). Methylthioadenosine (MTA) is also generated. One molecule of spermidine and two molecules of glutathione are then conjugated *via* trypanothione synthetase to generate trypanothione (Maya *et al.*, 2014).

To our knowledge, no reports have been published on selective inhibitors of *T. cruzi* spermidine synthase (TcSpdSyn), although substrate-mimicking inhibitors of SpdSyn have been investigated. *S*-Adenosyl-1,8-diamino-3-thio-octane (AdoDATO; Fig. 1) is a transition-state analogue that exhibits potent inhibitory activity against mammalian, trypanosomal and bacterial SpdSyn (Pegg *et al.*, 1995; Coward & Pegg, 1987). In addition, *trans*-4-methylcyclohexylamine (4MCHA) also exhibits moderate inhibitory activity towards SpdSyn (Fig. 1; Shirahata *et al.*, 1988). Crystal structures of *Plasmodium falciparum* spermidine synthase (PfSpdSyn) in complex with these inhibitors revealed the mechanisms of inhibition (Dufe *et al.*, 2007). AdoDATO simultaneously occupies the dcSAM-binding and the putrescine-binding pockets and appears to be competitive against both dcSAM and putrescine. In contrast, 4MCHA only occupies the putrescine-binding pocket in combination with dcSAM and appears to be competitive against putrescine and noncompetitive against dcSAM. Recently, novel inhibitors of PfSpdSyn have been investigated. Virtual screening followed by nuclear magnetic resonance (NMR) identified 5-(1*H*-benzimidazol-2-yl)pentan-1-amine (BIPA) as a strong binder of PfSpdSyn (Jacobsson *et al.*, 2008). The crystal structure of PfSpdSyn in complex with BIPA revealed a novel binding mode in which the benzimidazole moiety of BIPA simultaneously occupies the binding site of the aminopropyl moiety of dcSAM and that of putrescine (Sprenger *et al.*, 2015).

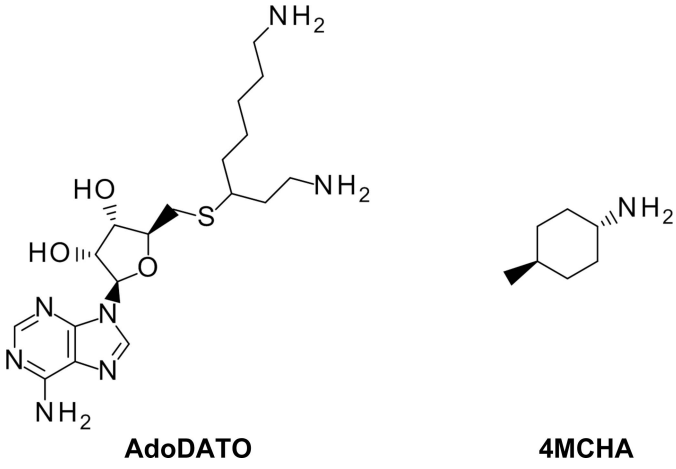

Figure 1
Known inhibitors of TcSpdSyn.

Over the last decade, fragment-based drug discovery (FBDD) has been developed as an effective approach to identifying novel drug candidates (Hubbard & Murray, 2011; Murray *et al.*, 2012). Several such candidates derived from FBDD are currently under clinical study (Baker, 2013). The first step in FBDD is identifying small-molecule ligands, which are called 'fragments' and generally have a molecular mass of less than 300 Da. As the fragments have low affinity for their target protein, the following biophysical methods are utilized to screen fragment libraries: surface plasmon resonance (SPR), NMR, thermal shift assay (TSA) and X-ray crystallography (Kranz & Schalk-Hihi, 2011; Lepre, 2011; Spurlino, 2011). X-ray crystallography and NMR are also required to validate the binding of fragments to the target protein and to determine the mode of binding. Promising fragment hits are selected based on structural information and then modified to occupy and strongly bind the pocket of the target protein (Abad *et al.*, 2011; Orita *et al.*, 2011).

Here, we used FBDD to identify selective inhibitors of TcSpdSyn. Fragment screening was first conducted, followed by X-ray crystallography. The crystal structures and novel mechanisms of inhibition are discussed below.

2. Materials and methods

2.1. Expression and purification

N-terminally His-tagged TcSpdSyn (Tc00.1047053510339.50) was expressed in *Escherichia coli* BL21(DE3) cells. The cells were grown in LB medium at 30°C to an OD_{600} of 0.7 and were then induced with 1 m*M* isopropyl *β*-D-1-thiogalactopyranoside. After 6 h, the cells were harvested and stored at −80°C. The harvested cells were resuspended and sonicated in lysis buffer (50 m*M* Tris–HCl pH 8.0, 500 m*M* NaCl, 5% glycerol, 5 m*M* imidazole, 10 m*M* *β*-mercaptoethanol, 1 m*M* phenylmethylsulfonyl fluoride). The lysate was centrifuged and the supernatant was loaded onto an Ni–NTA Superflow column (Qiagen, Valencia, California, USA) equilibrated with buffer *A* (50 m*M* Tris–HCl pH 8.0, 500 m*M* NaCl, 5% glycerol, 20 m*M* imidazole, 10 m*M* *β*-mercaptoethanol). The column was washed with buffer *A* and the protein was eluted with 250 m*M* imidazole. The buffer was then exchanged to buffer *B* (20 m*M* Tris–HCl pH 8.0, 1 m*M* DTT) by repeated ultrafiltration. The protein solution was loaded onto a Resource Q anion-exchange column (GE Healthcare, Cleveland, Ohio, USA) and eluted with a 0–1 *M* NaCl gradient. Fractions containing TcSpdSyn were collected and further purified using a Superdex 75 size-exclusion column (GE Healthcare) with buffer *C* (20 m*M* Tris–HCl pH 8.0, 150 m*M* NaCl). Purified protein was concentrated to 25 mg ml^{-1} in 20 m*M* Tris–HCl pH 8.0 buffer. For enzyme assays, N-terminally His-tagged

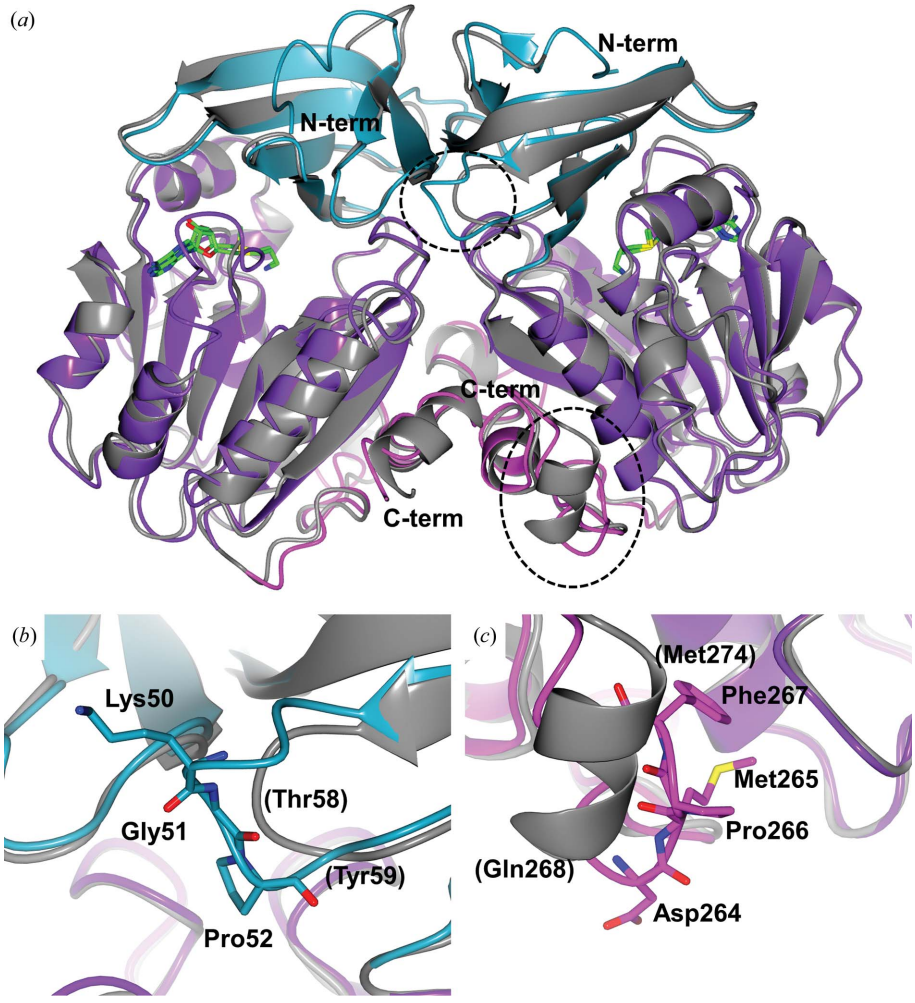

Figure 2
Comparison of TcSpdSyn and HsSpdSyn. (*a*) Ribbon diagram showing superimposed dimers of TcSpdSyn and HsSpdSyn. The N-terminal domain of TcSpdSyn is shown in cyan, the central core domain in purple and the C-terminal domain in magenta. HsSpdSyn is shown in grey. dcSAM is shown as a green stick model. (*b*, *c*) Close-up views of the differences between TcSpdSyn and HsSpdSyn in the N-terminal (*b*) and C-terminal (*c*) domains. Amino-acid labels for HsSpdSyn are given in parentheses.

human spermidine/spermine N^1-acetyltransferase 1 (SSAT1) was expressed and purified as described previously (Zhu *et al.*, 2006). The N-terminal His tag was cleaved with thrombin protease and removed using an Ni–NTA Superflow column (Qiagen).

2.2. TcSpdSyn binding assay

A Biacore 4000 system (GE Healthcare) was used for SPR assays. TcSpdSyn was immobilized on a CM7 sensor chip (GE Healthcare) by a standard amine-coupling method. Immobilization was performed with 100 µ*M* *S*-(5′-adenosyl)-3-thiopropylamine (Sigma–Aldrich, St Louis, Missouri, USA). Binding assays were performed at 25°C with running buffer consisting of HBS-P+ (GE Healthcare), 2% DMSO, 1 m*M* DTT, 12.5 µ*M* dcSAM (Peptide Institute, Osaka, Japan) and each fragment at a final concentration of 250 µ*M*.

TSAs were performed with a reaction solution consisting of 10 m*M* HEPES pH 7.4, 150 m*M* NaCl, 5× SYPRO Orange (Life Technologies, Carlsbad, California, USA), 0.05 mg ml^{-1} TcSpdSyn, 4 m*M* dcSAM (Peptide Institute) and each fragment at a final concentration of 2 m*M*. The reaction was carried out in a 384-well PCR plate using a CFX384 real-time PCR instrument (Bio-Rad Laboratories, Richmond, California, USA). In each plate, wells containing the reaction solution without fragments were monitored simultaneously as a negative control. After incubation at 25°C for 1 min, the temperature was increased from 25 to 80°C in 0.5°C increments with an equilibration time of 10 s at each temperature and fluorescence was monitored. The denaturation curves and T_m values were determined using the *CFX Manager* software (Bio-Rad Laboratories). T_m values were compared with negative-control wells to judge whether or not the fragments increased the thermal stability of TcSpsSyn–dcSAM.

2.3. TcSpdSyn inhibition enzyme assay

The inhibitory activities of compounds were examined using an enzyme-coupled assay incorporating SSAT1, which catalyzes the transfer of the acetyl group from acetyl-coenzyme A to spermidine. 7-Diethylamino-3-(4′-maleimidylphenyl)-4-methylcoumarin (Thermo Fisher Scientific, Waltham, Massachusetts, USA) was used to detect coenzyme A generated by SSAT1. Briefly, the following reaction mixture was incubated with or without compounds for 30 min at room temperature: 50 m*M* 4-(2-hydroxyethyl)-1-piperazineethanesulfonic acid (HEPES) pH 7.5, 10 µ*M* ethylenediaminetetraacetic acid (EDTA), 0.01%(*v*/*v*) Tween 20, 143 n*M* TcSpdSyn, 50 µ*M* dcSAM (Peptide Institute), 50 µ*M* putrescine (Sigma–Aldrich), 15 µ*M* acetyl-coenzyme A (Sigma–Aldrich) and 0.83 n*M* SSAT1. The fluorescence signal was then measured in a plate reader (Paradigm; Molecular Devices LLC, Sunnyvale, California, USA) with excitation at 405 nm and emission at 510 nm. The IC_{50} values were the mean of two independent experiments. For reference, 4MCHA was assayed and showed an IC_{50} value of 1.7 µ*M*.

2.4. Crystallization, data collection and refinement

Co-crystals of TcSpdSyn were obtained *via* the sitting-drop vapour-diffusion method. Before crystallization, 15 mg ml^{-1}

Table 1
Data-processing and refinement statistics.

Values in parentheses are for the outer shell.

Compound	dcSAM	dcSAM + 4MCHA	dcSAM + fragment 1	dcSAM + fragment 2	dcSAM + fragment 3	dcSAM + fragment 4	dcSAM + fragment 5	dcSAM + fragment 6
PDB code	4yuv	4yuw	4yux	4yuy	4yuz	4yu0	4yu1	4yu2
Space group	$P2_1$	$P2_12_12$	$P2_1$	$P2_1$	$P2_1$	$P2_1$	$P2_1$	$P2_1$
Unit-cell parameters								
a (Å)	44.4	95.2	44.8	44.8	43.5	43.6	43.4	43.7
b (Å)	92.4	141.2	93.9	94.1	99.7	99.8	99.3	100.3
c (Å)	68.3	43.7	68.0	68.2	134.6	135.0	135.1	71.4
α (°)	90	90	90	90	90	90	90	90
β (°)	99.8	90	100.2	100.4	91.7	90.6	90.5	107.7
γ (°)	90	90	90	90	90	90	90	90
Resolution (Å)	24.71–1.60 (1.64–1.60)	31.39–1.97 (2.02–1.97)	24.84–1.60 (1.64–1.60)	31.58–1.58 (1.62–1.58)	29.73–1.97 (2.02–1.97)	29.61–1.95 (2.00–1.95)	34.15–1.85 (1.90–1.85)	26.66–2.17 (2.23–2.17)
Multiplicity	3.5 (3.3)	6.0 (5.7)	3.6 (3.4)	3.7 (3.2)	3.4 (3.0)	3.4 (3.3)	3.6 (3.5)	3.4 (3.4)
Average $I/\sigma(I)$	14.0 (3.4)	37.9 (14.6)	10.0 (4.0)	38.6 (9.6)	35.5 (8.5)	26.5 (4.3)	23.5 (3.1)	8.6 (1.6)
$R_{\rm merge}$† (%)	6.0 (15.7)	7.4 (15.6)	5.9 (11.3)	10.4 (22.2)	14.9 (25.4)	6.9 (35.5)	6.9 (44.6)	7.1 (35.0)
No. of reflections	65545 (4971)	39164 (2741)	62982 (4859)	71049 (5283)	74896 (5204)	76898 (5559)	92299 (6826)	28723 (2122)
Completeness (%)	96.8 (99.9)	97.2 (94.0)	91.1 (95.8)	98.8 (99.2)	97.6 (92.7)	96.3 (94.9)	99.5 (99.5)	97.5 (98.4)
$R_{\rm work}$‡ (%)	19.6	18.5	17.8	19.8	20.0	20.9	19.6	22.0
$R_{\rm free}$§ (%)	24.2	23.3	21.8	23.6	25.0	25.3	24.5	28.2
Average B factor (Å^2)								
Protein	21.6	12.8	18.6	17.0	30.9	29.1	24.7	37.4
dcSAM	17.3	13.9	14.8	13.3	35.1	31.6	28.4	36.9
Ligand	—	11.3	19.4	24.2	40.4	32.8	43.0	45.2
Water	27.5	18.8	25.4	24.3	32.5	30.0	28.3	32.3
R.m.s.d., bond lengths (Å)	0.023	0.019	0.024	0.022	0.018	0.019	0.018	0.015
R.m.s.d., bond angles (°)	2.302	1.994	2.283	2.206	1.978	2.057	2.000	1.943
Ramachandran plot (%)								
Preferred	95.6	96.2	95.5	95.4	96.1	96.4	96.0	95.0
Allowed	3.8	3.1	3.6	4.1	3.3	3.0	3.3	4.6
Outliers	0.5	0.7	0.9	0.5	0.6	0.6	0.6	0.4

† $R_{\rm merge} = \sum_{hkl}\sum_i |I_i(hkl) - \langle I(hkl)\rangle| / \sum_{hkl}\sum_i I_i(hkl)$, where $I_i(hkl)$ is the intensity of an individual reflection and $\langle I(hkl)\rangle$ is the mean intensity obtained from multiple observations of symmetry-related reflections. ‡ $R_{\rm work} = \sum_{hkl} ||F_{\rm obs}| - |F_{\rm calc}|| / \sum_{hkl} |F_{\rm obs}|$. § A randomly omitted 5% of reflections were used for $R_{\rm free}$

TcSpdSyn was mixed with dcSAM to a final concentration of 2 m*M*. For co-crystallization with compounds, each compound was added to the mixture of TcSpdSyn and dcSAM to a final concentration of 5 m*M*. The reservoir solution consisted of 100 m*M* bis-tris pH 5.5–6.5, 200 m*M* ammonium sulfate, 10–15%(*w*/*v*) PEG 4000. Precipitated crystals were transferred into artificial mother liquor containing 20%(*v*/*v*) glycerol as a cryoprotectant and flash-cooled in liquid nitrogen. X-ray diffraction data were collected on the AR-NE3A beamline at the Photon Factory using a robotic sample changer and an automated data-collection system (Hiraki *et al.*, 2008, 2013; Yamada *et al.*, 2009). The structure was resolved by molecular replacement using *Phaser* (McCoy *et al.*, 2007). The apo structure of TcSpdSyn (PDB entry 3bwb; Structural Genomics of Pathogenic Protozoa Consortium, unpublished work) was used as a search model, and the disordered portion of the model was manually reconstructed using *Coot* (Emsley & Cowtan, 2004). After rigid-body refinement and restrained refinement using *REFMAC* (Murshudov *et al.*, 2011), dcSAM and each compound were clearly observed and fitted into the electron-density maps using *AFITT* (OpenEye Scientific Software, Santa Fe, New Mexico, USA). Dictionaries for dcSAM and compounds were generated using *AFITT* and structural refinement was conducted using *REFMAC*. The final structures were deposited in the PDB. Data-processing and refinement statistics are given in Table 1.

3. Results and discussion

3.1. Comparison of TcSpdSyn and HsSpdSyn

The crystal structure of TcSpdSyn in complex with dcSAM was determined at a resolution of 1.6 Å (Fig. 2*a*). TcSpdSyn formed a homodimer, and dcSAM bound to both monomer chains of the homodimer. The overall structure was similar to that of human spermidine synthase (HsSpdSyn; Wu *et al.*, 2007), which consists of an N-terminal β-sheet domain, a central core domain and a C-terminal domain (Wu *et al.*, 2007). Distinct differences between TcSpdSyn and HsSpdSyn were observed in the N-terminal and C-terminal domains. In the structure of TcSpdSyn, the three amino-acid residues Lys50, Gly51 and Pro52 were inserted between Thr58 and Tyr59 of HsSpdSyn (corresponding to Pro49 and Trp53 of TcSpdSyn). As shown in Fig. 2(*b*), these three residues were exposed to solvent. In the C-terminal domain, HsSpdSyn contained a short α-helix from Gln268 to Met274, whereas TcSpdSyn contained Pro266 and no α-helix was formed in this region. As shown in Fig. 2(*c*), this region was also exposed to solvent. Both of these two regions are exposed to the solvent,

thus the differences between TcSpdSyn and HsSpdSyn in the N-terminal and C-terminal domains are not considered to influence the structure of the central core domain, including the catalytic pocket.

Previously determined structures of HsSpdSyn revealed a flexible 'gatekeeping' loop composed of amino acids 174–182 (Wu *et al.*, 2007). In the HsSpdSyn–MTA structure, the gatekeeping loop is still flexible. On the other hand, the binding of putrescine/spermidine to HsSpdSyn–MTA stabilized the conformation of this loop and facilitated the formation of the active pocket. Asp176 in this loop formed a hydrogen bond to either the N^4-amino group of putrescine or the N^8-amino group of spermidine. This hydrogen bond might be a key interaction in the formation of the active pocket. Similarly, TcSpdSyn also contains a gatekeeping loop, which is composed of amino acids 169–177. The gatekeeping loop is disordered in the apo structure of TcSpdSyn (PDB entry 3bwb; Structural Genomics of Pathogenic Protozoa Consortium, unpublished work). However, in the present study the gatekeeping loop can be clearly observed in the structure of TcSpdSyn bound to dcSAM (Fig. 3*a*). The gatekeeping loop of TcSpdSyn is therefore stabilized upon the binding of dcSAM. The conformations of the side chain of Asp171 in the loop, corresponding to Asp176 of HsSpdSyn, differ between chains *A* and *B*. The side chain of Asp171 in chain *A* is orientated towards the outside of the pocket, whereas that in chain *B* is orientated towards the inside of the pocket. This suggests that the structure of the pocket is not completely stabilized by dcSAM. Of note, the binding mode of dcSAM in TcSpdSyn is similar to that in HsSpdSyn: the adenine ring forms hydrogen bonds to Asp149, Pro175 and the main-chain NH of Gly150, the ribose hydroxyls form hydrogen bonds to Gln40 and Asp118, and the aminopropyl NH_2 forms hydrogen bonds to Asp98 and Asp168 (Fig. 3*b*).

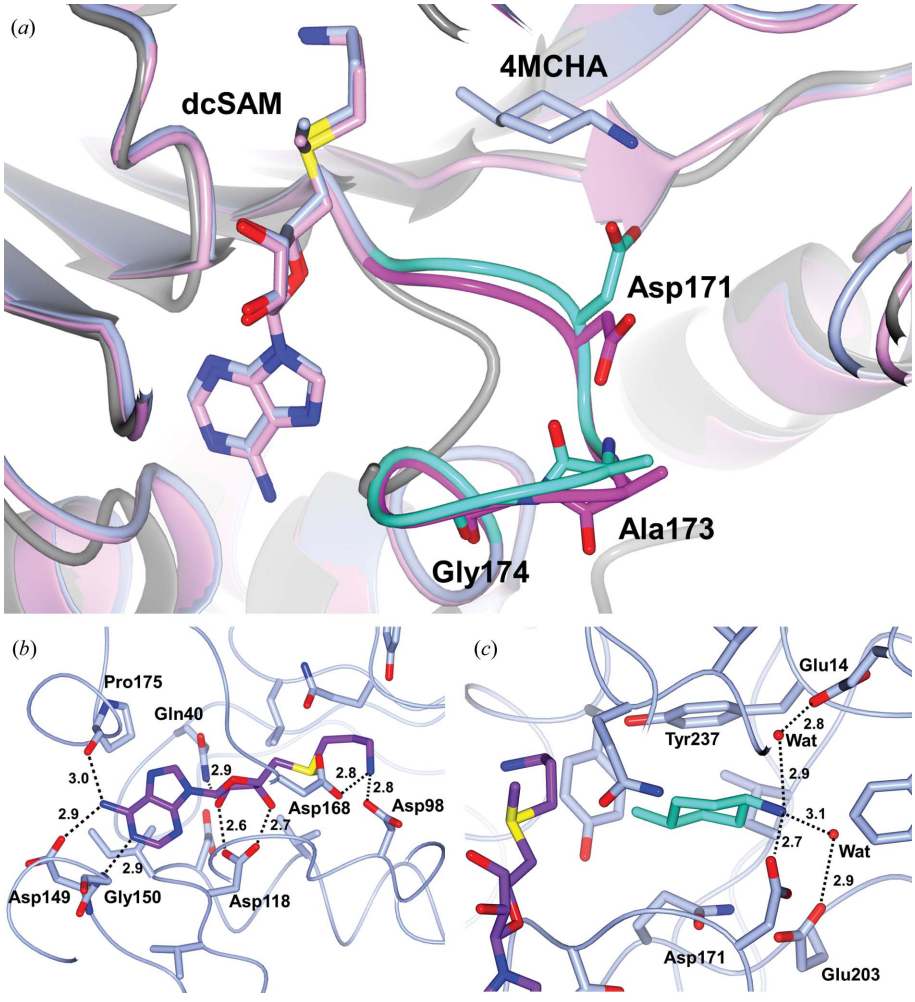

Figure 3
(*a*) Superimposition of the apo form of TcSpdSyn (PDB entry 3bwb), TcSpdSyn–dcSAM and TcSpdSyn–dcSAM–4MCHA. dcSAM and 4MCHA are shown as stick models. Protein structures are shown as ribbon diagrams. The apo form is shown in grey, TcSpdSyn–dcSAM in pink and TcSpdSyn–dcSAM–4MCHA in light blue. The gatekeeping loops of TcSpdSyn–dcSAM and TcSpdSyn–dcSAM–4MCHA are shown in cyan and magenta, with stick models of Asp171, Ala173 and Gly174. (*b*) The binding mode of dcSAM in TcSpdSyn–dcSAM. dcSAM is shown as a purple stick model. Residues that interact with dcSAM are shown as light blue stick models. (*c*) The binding mode of 4MCHA in TcSpdSyn–dcSAM–4MCHA. 4MCHA is shown as a cyan stick model indicates. Residues that interact with 4MCHA are shown as light blue stick models. Hydrogen bonds are indicated by dashed lines with bond distances in Å.

We conducted primary fragment screening using TSAs and SPR assays. The initial purpose of fragment screening was to identify novel inhibitors that bind to the putrescine-binding pocket, as dcSAM binds tightly in the pocket and the fragments do not fully occupy the dcSAM-binding pocket. According to the results of structural analysis, TSAs and SPR assays were carried out in the presence of dcSAM to identify fragment hits that bind in the putrescine-binding pocket stabilized by dcSAM. TSAs and SPR assays were performed with a single concentration

of each fragment to clarify whether or not the fragments are likely to bind TcSpdSyn. We selected fragment hits that had been confirmed to increase the T_m value of TcSpdSyn–dcSAM in TSAs and/or to bind TcSpdSyn–dcSAM in SPR assays. Subsequently, co-crystal structures of TcSpdSyn–dcSAM in complex with fragment hits were solved and the inhibitory activities of fragment hits were evaluated by enzyme assays. In this paper, we report the co-crystal structures of fragments 1–6 (Fig. 4). Fragments 1–6 inhibit TcSpdSyn in a dose-dependent manner (data not shown) and IC_{50} values were calculated. Fig. 4 shows OMIT $F_o - F_c$ maps of fragments, in which all of the fragments were clearly observed. In the following sections, we discuss binding sites, binding modes and inhibition mechanisms of fragment hits.

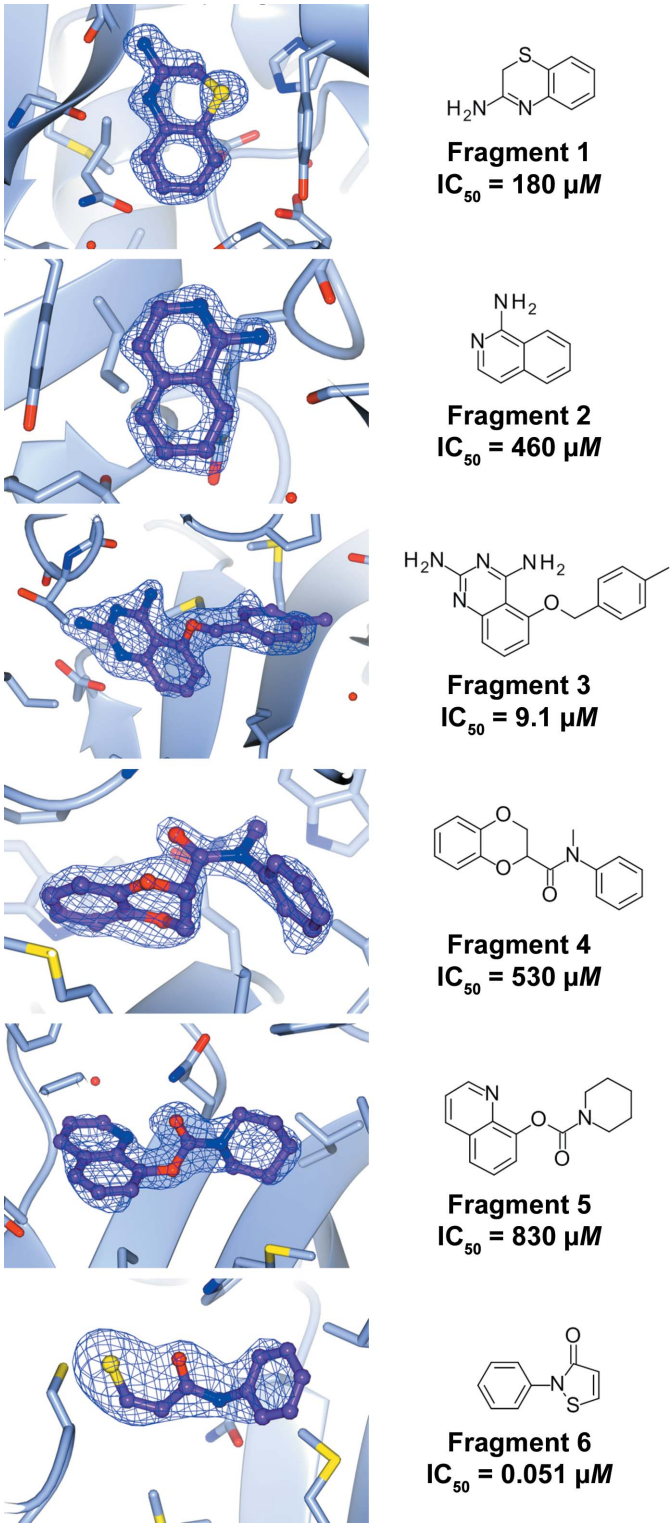

Figure 4
OMIT $F_o - F_c$ map and chemical structures of fragments 1–6 (contoured at 2.5σ). The fragments are shown as purple ball-and-stick models, while the protein is shown as a light blue ribbon diagram and stick model. The IC_{50} values of TcSpdSyn enzyme assays are also shown.

3.2. Fragments bound in the putrescine-binding pocket

The crystal structures of fragment hits that bound to TcSpdSyn revealed two fragment-binding sites. The first was the putrescine-binding pocket, as expected, and the second was the dimer interface (Fig. 5). Fragment hits 1 and 2 were identified in the putrescine-binding pocket. Both fragments were recognized *via* an 'induced-fit' mechanism of the putrescine-binding pocket (Fig. 6*a*). Tyr237 flipped down, thereby exposing the side chains of Asp69 and Thr236 and the main-chain O atoms of Ile63, Gln64 and Thr236 to the pocket. The amino group of fragment 1 formed hydrogen bonds to the side-chain and the main-chain O atoms of Thr236 (Fig. 6*b*). In addition, fragment 1 formed a hydrogen bond to a water molecule that binds to the side chain of Asp69. The N atom of the thiazine ring was most likely protonated and acted as a hydrogen donor for the hydrogen bond to Ile63. The benzene ring of fragment 1 formed van der Waals and hydrophobic interactions with the propyl group of dcSAM. Fragment 2 also formed hydrogen bonds to the main-chain O atoms of Ile63 and Thr236 (Fig. 6*c*). The benzene ring of fragment 2 formed

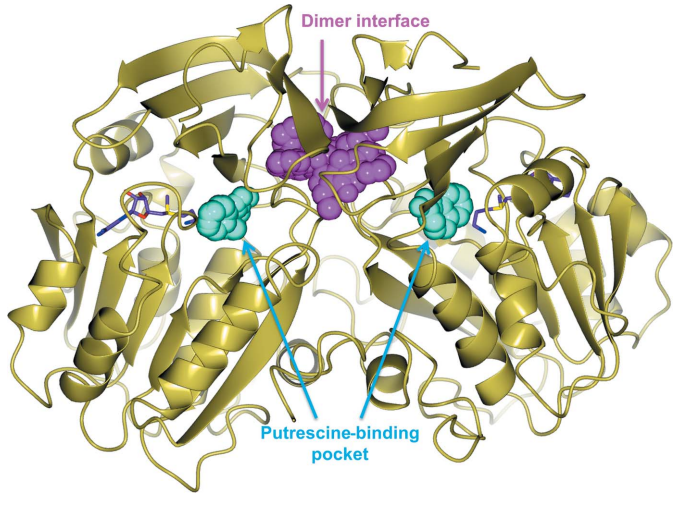

Figure 5
Overview of fragment-binding sites. TcSpdSyn is shown as a ribbon diagram. dcSAM is shown as a purple stick model, fragments bound in the putrescine-binding pocket are shown as cyan space-filling models and model fragments bound in the dimer interface are shown as magenta space-filling models.

van der Waals and hydrophobic interactions with the propyl group of dcSAM in the same manner as fragment 1. Although neither fragment interacted with Asp171, the conformation of the gatekeeping loop was similar to that in the structure of TcSpdSyn–dcSAM–4MCHA, but not to that in the structure of TcSpdSyn–dcSAM (Fig. 6*d*). Briefly, in the structures with fragments 1 and 2 bound the side chain of Asp171 is oriented towards the inside of the putrescine-binding pocket and the conformation of the peptide bond between Ala173 and Gly174 is almost identical to that of the 4MCHA-bound structure. These findings suggest that stabilization of the gatekeeping loop does not require interactions with Asp171, but instead requires occupancy of the putrescine-binding pocket. Fragments 1 and 2 did not exhibit potent inhibitory activities (IC_{50} values of 180 and 460 μM, respectively). However, the ligand efficiency (LE) values of fragments 1 and 2 were sufficient for use in FBDD (0.46 and 0.41, respectively). In addition, the expansion of the pocket by an induced-fit mechanism resulted in space surrounding fragments 1 and 2. Fragments 1 and 2 are therefore promising fragment hits for further development and optimization *via* chemical synthesis.

3.3. Fragments bound in the dimer interface

Contrary to our expectations, fragments 3–6 bound to the interface of the TcSpdSyn homodimer. In the structures with fragments 3, 4 or 5 bound, one molecule of each fragment formed noncovalent interactions with the interface (Figs. 7*a*, 7*b* and 7*c*). If the interface were completely symmetrical, two molecules of the fragment should be observed in the interface with occupancies of 0.5. However, crystal packing might disorder the symmetry and result in the appearance of only a single molecule. On the other hand, two molecules of fragment 6 formed covalent bonds with the interface (Fig. 7*d*).

Fragment 3 formed four hydrogen bonds to amino-acid residues from one monomer of the dimer interface (Fig. 7*a*). The N1 atom and the amino group at the 2-position of quinazoline formed hydrogen bonds to the side chain of

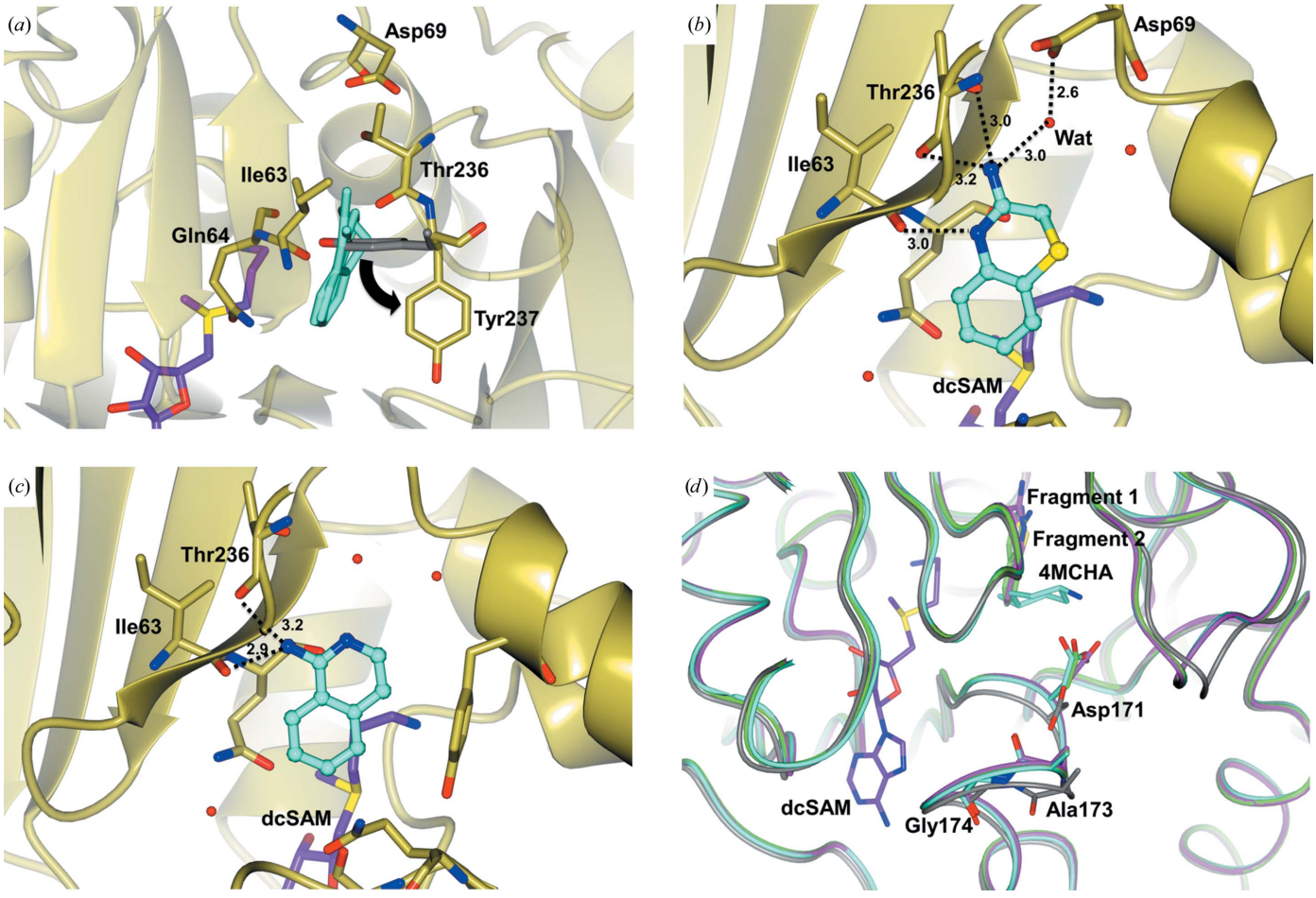

Figure 6
(*a*, *b*, *c*) Binding modes of fragments bound in the putrescine-binding pocket. In each figure, fragments 1 and 2 are shown in cyan, dcSAM in blue and water molecules as red balls. TcSpdSyn is shown as as a gold ribbon diagram and stick model. (*a*) Induced fit upon binding of fragments. The side chain of Tyr237 in TcSpdSyn–dcSAM is shown as a grey stick model. (*b*, *c*) Binding modes of fragments 1 (*b*) and 2 (*c*). Hydrogen bonds are indicated by dashed lines with bond distances in Å. (*d*) Superimposition of TcSpdSyn–dcSAM (grey), TcSpdSyn–dcSAM–4MCHA (cyan), TcSpdSyn–dcSAM–fragment 1 (magenta) and TcSpdSyn–dcSAM–fragment 2 (green).

Glu14. The amino group at the 2-position of quinazoline also formed a hydrogen bond to the O atom of the main chain of Thr236. The amino group at the 4-position of quinazoline formed hydrogen bonds to the O atom of the main chain of Pro235. The benzene ring of quinazoline and the *S*-methyl group of Met24 formed a CH–π interaction. The methylbenzyl group also formed a CH–π interaction with Pro238 from another monomer in the dimer interface. Fragments 4 and 5 exhibited similar binding modes (Figs. 7*b* and 7*c*). The O atom of the carboxamide in fragment 4 and that of the carbamate in fragment 5 formed hydrogen bonds to the main-chain NH of Cys239. The benzodioxine in fragment 4 and the quinoline in fragment 5 formed a van der Waals interaction with the plane-like surface of Pro238. Of these three fragments, fragment 3 exhibited the most potent inhibitory activity, with an IC_{50} value of 9.1 μM. In contrast, the IC_{50} values of fragments 4 (530 μM) and 5 (830 μM) were more than 50 times that of fragment 3. This marked difference appears to be related to differences in binding mode. The strong affinity with the dimer interface might therefore result in potent inhibitory activities.

The binding mode of fragment 6 also demonstrates the relationship between inhibitory activity and binding affinity with the dimer interface. The molecular mass of fragment 6 is smaller than those of fragments 3–5 and two molecules of fragment 6 bind the interface. The isothiazolone ring of fragment 6 is opened by the thiol group of Cys239 and a disulfide bond is formed. As enzyme assays and co-crystallization were performed under nonreducing conditions, the disulfide bond with Cys239 might also form in enzyme assays. Isothiazolone has been shown to make a disulfide bond with the thiol group of cysteine (Hayakawa *et al.*, 1999; Trevillyan *et al.*, 1999); however, the six cysteine residues other than Cys239 were not modified by fragment 6 in the crystal structure. Thus, fragment 6 specifically binds the dimer interface and makes a disulfide bond with Cys239. This disulfide bond might result in highly potent inhibition of TcSpdSyn by fragment 6 (IC_{50} value of 0.051 μM).

3.4. Allosteric inhibition mechanism

To identify the mechanism behind the potent inhibition by fragment 6, we conducted a detailed analysis of the crystal

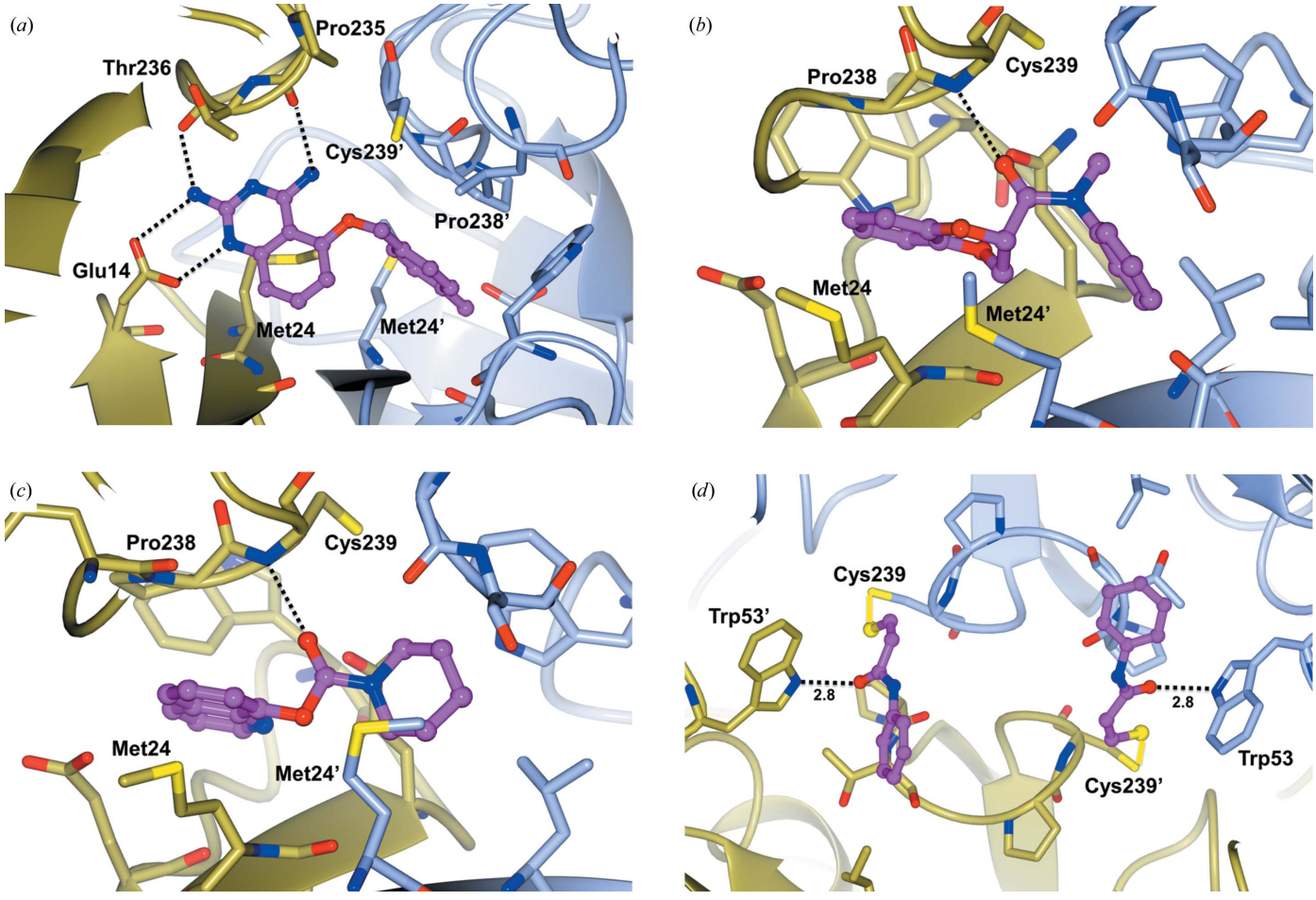

Figure 7
Binding modes of fragments bound in the dimer interface: (*a*) fragment 3, (*b*) fragment 5, (*c*) fragment 5 and (*d*) fragment 6. Fragments 3–6 are shown as magenta ball-and-stick models, while the monomers of TcSpdSyn are shown in gold and light blue. Primes indicate amino-acid residues from the opposite monomer. Hydrogen bonds are indicated by dashed lines with bond distances in Å. Yellow lines indicate disulfide bonds.

structures. In the TcSpdSyn–dcSAM–4MCHA structure, the distance between the S atom of Cys239 and the O atom of the side chain of Gln22 was 3.5 Å (Fig. 8*a*), which corresponds to a sulfur–oxygen interaction. Gln22 was at the N-terminal end of the β-strand that formed the β-sheet spanning two monomers. The loop from Asn16 to Gln22 facilitated the formation of the putrescine-binding pocket. The side chain of Gln18 formed hydrogen bonds to the main-chain NH of Ala173 in the gatekeeping loop and the side chain of Asn16. Furthermore, Trp19 formed van der Waals interactions with the side chain of Asp171, which recognized the amine group of putrescine. The amino-acid sequences of SpdSyn from *T. cruzi*, *T. brucei*, *Leishmania major*, *Plasmodium falciparum*, human and mouse were aligned (see Supplementary Fig. S1). Only *Trypanosoma* conserves all of the key residues Asn16, Gln18, Trp19, Gln22, Asp171 and Cys239. Therefore, the stabilization mechanism described above is unique to *Trypanosoma*.

Fragment 6 clearly disrupted the interaction between Gln22 and Cys239 *via* the covalent modification of Cys239 (Fig. 8*b*).

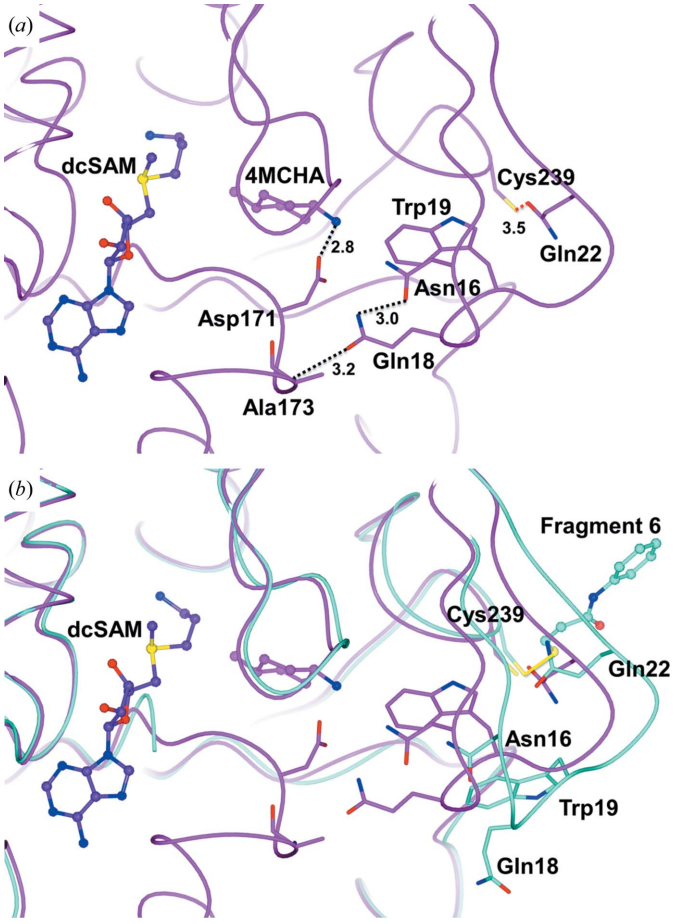

Figure 8
(*a*) Interactions between the N-terminal domain and the putrescine-binding pocket in the TcSpdSyn–dcSAM–4MCHA structure. Red dashed lines indicate sulfur–oxygen interactions and black lines indicate hydrogen bonds. Bond distances are shown in Å. (*b*) Superimposition of the TcSpdSyn–dcSAM–4MCHA structure and the fragment 6-bound structure. TcSpdSyn–dcSAM–4MCHA is shown in magenta and TcSpdSyn–dcSAM–fragment 6 is shown in cyan. Yellow lines indicate covalent bonds.

Gln22 moved away from Cys239 and the loop from Asn16 to Gln22 underwent drastic conformational changes. The loop moved away from the putrescine-binding pocket, and the side chain of Gln18 was orientated towards the solvent. As a result, the gatekeeping loop was disordered and the putrescine-binding pocket did not form. These findings suggest that the interaction between Gln22 and Cys239 is required to form the

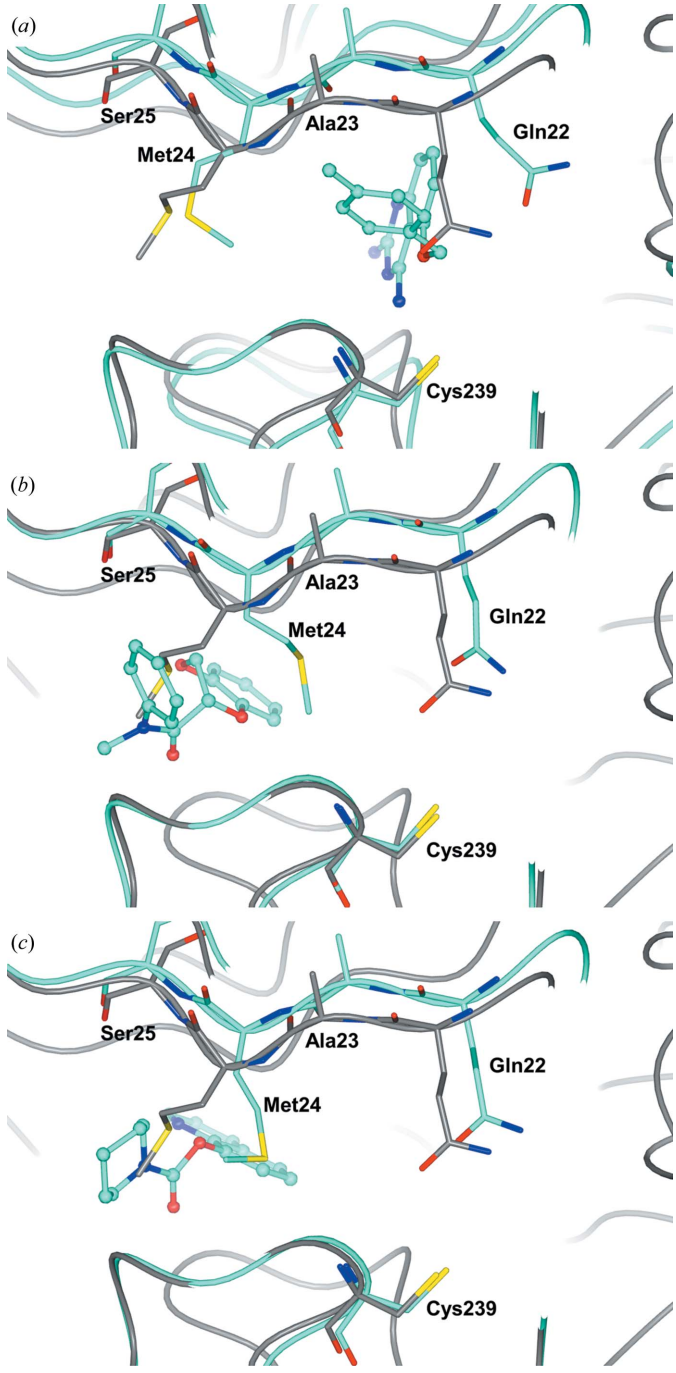

Figure 9
Disruption of the interaction between Gln22 and Cys239 on the binding of fragments 3 (*a*), 4 (*b*) and 5 (*c*). Fragments are shown as cyan ball-and-stick models. Fragment-bound structures are shown in cyan. The TcSpdSyn–dcSAM–4MCHA structure is shown in grey.

putrescine-binding pocket. Disruption of this interaction might therefore inhibit enzyme activity.

Regarding compounds that form noncovalent bonds with the dimer interface, fragment 3 obstructed Gln22 and in turn its interaction with Cys239 (Fig. 9*a*). Fragments 4 and 5 moved the side chain and the main chain of Met24 and bound in the vacant space. Although Ser25 did not move notably, Ala23 and Gln22 moved, as well as Met24. As a result, the interaction between Gln22 and Cys239 was disrupted (Figs. 9*b* and 9*c*). In the structures with fragments 3–5 bound, the gatekeeping loops were disordered and the putrescine-binding pockets did not form. This is consistent with the fragment 6-bound structure.

Based on these facts, the conformation of the residues from Gln22 to Met24 plays an important role in the formation of the putrescine-binding pocket. These residues affect the conformation of the Asn16–Gln22 loop that makes a hydrogen-bond network and van der Waals interactions with the gatekeeping loop. Binding of the fragments to the dimer interface adjacent to Gln22–Met24 changes their conformation and results in prevention of the formation of the putrescine-binding pocket.

4. Conclusion

In the present study, we first determined the crystal structures of TcSpdSyn–dcSAM and TcSpdSyn–dcSAM–4MCHA. The gatekeeping loop of TcSpdSyn was stabilized upon the binding of dcSAM and the putrescine-binding pocket completely formed upon the binding of 4MCHA, which is a mimic of putrescine. The structure of the putrescine-binding pocket is also supported by the loop in the N-terminal domain, which composes the interface of the TcSpdSyn homodimer. Crystal structures of TcSpdSyn in complex with fragment hits revealed two novel inhibition mechanisms: induced fit in the putrescine-binding pocket and allosteric inhibition at the dimer interface. The putrescine-binding pocket was expanded by an induced-fit mechanism, which enables further modification of fragments to achieve potent inhibitory activities *via* occupation of the extended pocket. Although the structural features of the putrescine-binding pocket are conserved between TcSpdSyn and HsSpdSyn when substrates bind, allosteric inhibition involves unconserved amino-acid residues. Allosteric inhibitors might therefore be highly selective for TcSpdSyn. The findings of the present study will help to facilitate the structure-based design of TcSpdSyn-selective and potent inhibitors as a promising therapy for Chagas disease.

Acknowledgements

We thank Drs Yutaka Akiyama, Masakazu Sekijima and Takashi Ishida at Tokyo Institute of Technology for selecting TcSpdSyn as a drug target. We thank Drs Kiyoshi Kita and Daniel Ken Inaoka at Tokyo University and Dr Kenji Hirayama at Nagasaki University for their helpful suggestions regarding trypanosomes. We thank Drs Koji Furukawa, Kazuhiko Yamasaki, Tomomi Kubota and Osamu Tani at the National Institute of Advanced Industrial Science and Technology for their valuable discussions regarding assay development. We thank Dr Toshiya Senda at the High Energy Accelerator Research Organization and the beamline staff of AR-NE3A for assisting in the collection and processing of X-ray diffraction data.

References

Abad, M. C., Gibbs, A. C. & Zhang, X. (2011). *Methods Enzymol.* **493**, 487–508.
Baker, M. (2013). *Nature Rev. Drug Discov.* **12**, 5–7.
Bern, C., Montgomery, S. P., Herwaldt, B. L., Rassi, A. Jr, Marin-Neto, J. A., Dantas, R. O., Maguire, J. H., Acquatella, H., Morillo, C., Kirchhoff, L. V., Gilman, R. H., Reyes, P. A., Salvatella, R. & Moore, A. C. (2007). *JAMA*, **298**, 2171–2181.
Centers for Disease Control and Prevention (2011). *Neglected Tropical Diseases.* http://www.cdc.gov/globalhealth/ntd/.
Centers for Disease Control and Prevention (2013). *Parasites – American Trypanosomiasis (also known as Chagas Disease).* http://www.cdc.gov/parasites/chagas/epi.html.
Colotti, G., Baiocco, P., Fiorillo, A., Boffi, A., Poser, E., Chiaro, F. D. & Ilari, A. (2013). *Future Med. Chem.* **5**, 1861–1875.
Coward, J. K. & Pegg, A. E. (1987). *Adv. Enzyme Regul.* **26**, 107–113.
Dufe, V. T., Qiu, W., Müller, I. B., Hui, R., Walter, R. D. & Al-Karadaghi, S. (2007). *J. Mol. Biol.* **373**, 167–177.
Emsley, P. & Cowtan, K. (2004). *Acta Cryst.* D**60**, 2126–2132.
Fairlamb, A. H., Blackburn, P., Ulrich, P., Chait, B. T. & Cerami, A. (1985). *Science*, **227**, 1485–1487.
Flohé, L., Hecht, H.-J. & Steinert, P. (1999). *Free Radic. Biol. Med.* **27**, 966–984.
Hayakawa, N., Nozawa, K., Ogawa, A., Kato, N., Yoshida, K., Akamatsu, K., Tsuchiya, M., Nagasaka, A. & Yoshida, S. (1999). *Biochemistry*, **38**, 11501–11507.
Hiraki, M., Watanabe, S., pHonda, N., Yamada, Y., Matsugaki, N., Igarashi, N., Gaponov, Y. & Wakatsuki, S. (2008). *J. Synchrotron Rad.* **15**, 300–303.
Hiraki, M., Yamada, Y., Chavas, L. M. G., Wakatsuki, S. & Matsugaki, N. (2013). *J. Synchrotron Rad.* **20**, 890–893.
Hubbard, R. E. & Murray, J. B. (2011). *Methods Enzymol.* **493**, 509–531.
Ikeguchi, Y., Bewley, M. C. & Pegg, A. E. (2006). *J. Biochem.* **139**, 1–9.
Jacobsson, M., Gäredal, M., Schultz, J. & Karlén, A. (2008). *J. Med. Chem.* **51**, 2777–2786.
Kranz, J. K. & Schalk-Hihi, C. (2011). *Methods Enzymol.* **493**, 277–298.
Krauth-Siegel, R. L. & Comini, M. A. (2008). *Biochim. Biophys. Acta*, **1780**, 1236–1248.
Lepre, C. A. (2011). *Methods Enzymol.* **493**, 219–239.
Manta, B., Comini, M., Medeiros, A., Hugo, M., Trujillo, M. & Radi, R. (2013). *Biochim. Biophys. Acta*, **1830**, 3199–3216.
Maya, J. D., Salas, C. O., Aguilera-Venegas, B., Diaz, M. V. & López-Muñoz, R. (2014). *Curr. Med. Chem.* **21**, 1757–1771.
McCoy, A. J., Grosse-Kunstleve, R. W., Adams, P. D., Winn, M. D., Storoni, L. C. & Read, R. J. (2007). *J. Appl. Cryst.* **40**, 658–674.
Murray, C. W., Verdonk, M. L. & Rees, D. C. (2012). *Trends Pharmacol. Sci.* **33**, 224–232.
Murshudov, G. N., Skubák, P., Lebedev, A. A., Pannu, N. S., Steiner, R. A., Nicholls, R. A., Winn, M. D., Long, F. & Vagin, A. A. (2011). *Acta Cryst.* D**67**, 355–367.
Orita, M., Ohno, K., Warizaya, M., Amano, Y. & Niimi, T. (2011). *Methods Enzymol.* **493**, 383–419.
Pegg, A. E., Poulin, R. & Coward, J. K. (1995). *Int. J. Biochem. Cell Biol.* **27**, 425–442.
Shirahata, A., Morohoshi, T. & Samejima, K. (1988). *Chem. Pharm. Bull.* **36**, 3220–3222.

Sprenger, J., Svensson, B., Hålander, J., Carey, J., Persson, L. & Al-Karadaghi, S. (2015). *Acta Cryst.* D**71**, 484–493.
Spurlino, J. C. (2011). *Methods Enzymol.* **493**, 321–356.
Trevillyan, J. M. *et al.* (1999). *Arch. Biochem. Biophys.* **364**, 19–29.
World Health Organization (2013). *Neglected Tropical Diseases.* http://www.who.int/neglected_diseases/diseases/en/.
World Health Organization (2015). *Chagas Disease (American Trypanosomiasis).* http://www.who.int/mediacentre/factsheets/fs340/en/.
Wu, H., Min, J., Ikeguchi, Y., Zeng, H., Dong, A., Loppnau, P., Pegg, A. E. & Plotnikov, A. N. (2007). *Biochemistry*, **46**, 8331–8339.
Yamada, Y. H. M., Sasajima, K., Matsugaki, N., Igarashi, N., Amano, Y., Warizaya, M., Sakashita, H., Kikuchi, T., Mori, T., Toyoshima, A., Kishimoto, S. & Wakatsuki, S. (2009). *AIP Conf. Proc.* **1234**, 415–418.
Zhu, Y.-Q., Zhu, D.-Y., Yin, L., Zhang, Y., Vonrhein, C. & Wang, D.-C. (2006). *Proteins*, **63**, 1127–1131.